HHS Public Access

Author manuscript

Am J Ophthalmol. Author manuscript; available in PMC 2021 October 01.

Published in final edited form as:

Am J Ophthalmol. 2020 October ; 218: 17–27. doi:10.1016/j.ajo.2020.05.006.

Quantitative Analysis of the Choriocapillaris in Uveitis Using en face Swept Source Optical Coherence Tomography Angiography

Zhongdi Chu, PhD[1], **Jessica E Weinstein, MD**[2], **Ruikang K Wang, PhD**[1,2], **Kathryn L Pepple, MD, PhD**[2]

[1]Department of Bioengineering, University of Washington, Seattle, WA 98195

[2]Department of Ophthalmology, University of Washington, Seattle, WA 98104

Abstract

Purpose: To perform a quantitative analysis of choriocapillaris (CC) flow deficits (FDs) in patients with uveitis.

Design: Retrospective cross-sectional study

Methods: Swept-source optical coherence tomography based angiography (SS-OCTA) macular volume scans (3×3 mm and 6×6 mm) were obtained using the PLEX® Elite 9000: *En face* CC images were generated and analyzed using an automated flow deficit identification algorithm. Three quantitative metrics were determined for each eye: FD number (FDN), mean FD size (MFDS), and FD density (FDD). Quantitative metrics were compared between uveitis and control eyes. The uveitis cohort was further subdivided by the presence or absence of choroidal involvement, and quantitative metrics were compared between subgroups and normal controls

Results: A total of 38 eyes from 38 controls and 73 eyes from 73 uveitis subjects were included in this study. Eyes with uveitis have significantly larger CC MFDS (3×3 mm, $p<0.0001$; 6×6 mm, $p<0.0001$) and higher FDD ($p=0.0002$; $p=0.0076$) when compared to control eyes. Additional analysis determined that these differences are due to the choroidal disease subgroup, which demonstrates significantly larger MFDS (3×3 =1108 μm^2; 6×6 =1104 μm^2) compared to both normal controls (752 μm^2, $p<0.0001$; 802 μm^2, $p<0.0001$) and uveitis patients without choroidal involvement (785 μm^2, $p<0.0001$; 821 μm^2, $p<0.0001$). No significant differences were found between the quantitative metrics of controls and patients without choroidal involvement.

Conclusions: Automated quantification of CC can identify pathological FDs and provide quantitative metrics describing such lesions in patients with uveitis. Posterior uveitis patients have significantly larger CC FDs than patients with other forms of uveitis.

Corresponding Author: Kathryn L Pepple, 908 Jefferson St, Seattle, WA, 98104, Phone: 206-897-4611, Fax: 206-897-4320, kpepple@u.washington.edu.

Automated analysis of en face SS-OCTA images identifies significant differences in choriocapillaris blood flow between patients with posterior uveitis and controls using three quantitative metrics.

Introduction

Optical coherence tomography (OCT) angiography (OCTA) is a non-invasive imaging modality that has demonstrated utility in studies of retinal vasculature disease.[1–9] In patients with uveitis, including intermediate, posterior and panuveitis, spectral domain OCTA (SD-OCTA) has identified both qualitative and quantitative retinal vasculature flow abnormalities.[3, 6, 10–13] However, in certain types of uveitis, such as birdshot chorioretinopathy or punctate inner choroidopathy, pathology may also involve or be entirely limited to the choroid and choriocapillaris (CC).[3, 6, 10, 14–18] While case reports and case series using SD-OCTA have identified CC flow abnormalities in patients with some forms of posterior uveitis, the vascular beds below the retinal pigmented epithelium (RPE) complex have not been thoroughly investigated and quantitative analysis of CC abnormalities is limited.[19–21]

The emergence of swept-source OCTA (SS-OCTA) technology allows for more in-depth characterization of choroidal blood flow in healthy and diseased eyes. SS-OCTA imaging can provide improved visualization of blood flow in the choroid and CC due to better depth penetration through the RPE/ Bruch's membrane(BM) complex and lower sensitivity roll-off when compared to SD-OCT systems.[22] Additionally, acquisition speeds of more than 100 kHz facilitate wide angle imaging,[23] a feature important for diseases like uveitis that frequently manifest clinically significant lesions in the extrafoveal macula. Finally, segmentation of SS-OCTA data into choroidal or CC *en face* slabs is showing promise for the detection of inflammatory disease activity without a need for fluorescein or indocyanine green based angiography.[15, 24–27] In order to bring these benefits of SS-OCTA imaging into more widespread clinical use, image acquisition will need to be coupled with automated image analysis for the rapid, reproducible, and quantitative detection of relevant disease associated abnormalities. Towards this goal, in this study, we test an automated *en face* CC OCTA image analysis approach for the ability to detect and quantify CC in patients with uveitis.

Methods

This single-institution retrospective cross-sectional study was approved by the Institutional Review Board at the University of Washington. Written informed consent regarding the nature of this research study was obtained for all subjects before imaging. This study was performed in accordance with the tenets of the Declaration of Helsinki and the Health Insurance Portability and Accountability Act of 1996.

Study Population

Patients 18 years or older, diagnosed with anterior, intermediate, posterior, panuveitis, or retinal vasculitis were recruited for SS-OCTA imaging between August 2016 and July 2018 at the University of Washington Harborview Medical Center Eye institute. Patients with active and inactive uveitis were recruited. Upon entry in the study, subject data including gender, age, uveitis diagnosis, and involvement of one or both eyes were collected. Diagnosis of anatomic location of uveitis and determination of location of disease activity were made using the criteria established by the standardization of uveitis nomenclature

(SUN) criteria based on clinical exam and additional imaging modalities such as color fundus, fluorescein angiography, indocyanine green angiography, SD-OCT, and fundus autofluorescence at the discretion of the examining physician.[28] Results of laboratory testing, chest X-ray, biopsy, or MRI imaging, when performed, were used to further classify uveitis diagnosis by underlying etiology.

Image acquisition and scanning protocols

Research imaging was performed on a 100kHz SS-OCTA PLEX® Elite 9000 (Carl Zeiss Meditec, Dublin, CA), with a central wavelength of 1060 nm, a bandwidth of 100 nm, axial resolution of ~6 μm and lateral resolution of ~20 μm in retinal tissue.[29] FastTrac motion tracking was used during all scans to minimize possible motion artifacts during imaging. 3×3 mm and 6×6 mm volume scans centered on the fovea were obtained for both eyes of all subjects. For unilateral cases, the diseased eye was selected for further analysis, and for bilateral cases, the eye with the highest signal strength was selected. If both eyes were equal in signal strength, then the right eye was used. Images with severe motion artifacts, macular edema, or signal strength lower than seven were excluded from further analysis.[30]

The commercially available PLEX® Elite algorithm was used to segment the CC and generate *en face* CC flow images. In brief, The RPE best fit line was determined using PLEX® Elite software, manual corrections were performed in the case of failed automated segmentation. The CC was defined as the region from 16–31 μm below the RPE.[31] The complex optical microangiography (OMAG^c) algorithm[32] was used to generate OCTA volumes, then maximum projection was applied to the segmented CC OCTA volumes to generate the *en face* images. After acquiring CC *en face* images, a previously published compensation strategy using structural OCT information was also applied through MATLAB (R2016b; MathWorks, Inc, Natick, Massachusetts, USA) to correct the OCTA flow in the CC images for signal attenuation.[33] Quantitative analysis was then performed on the *en face* image.

Definition and quantification of choriocapillaris flow deficits

In this study the term “flow deficit (FD)” is used to describe areas where there is a lack of the flow or flow below the detectable threshold of OCTA.[34, 35] In normal controls, these areas are believed to represent the CC vascular walls and inter-capillary spaces. In disease states, these areas are believed to represent choroidal non-perfusion, or the presence of choroidal infiltrates leading to blood flow that is below the OCTA detection sensitivity. The similar term flow void has been used in other reports[36–38] and is well-described in the literature.[39] FDs were defined on each *en face* image using a custom algorithm through MATLAB (R2016b; MathWorks, Inc, Natick, Massachusetts, USA) employing a comprehensive thresholding strategy.[34] This method is summarized in Figure 1. In brief, for each *en face* CC slab, a complex thresholding algorithm that utilizes fuzzy C-means clustering was applied. Pixels that self-cluster into the lowest intensity group were segmented as the initial FDs. The image was then binarized such that areas of CC flow are bright and the areas of absent flow (FDs) are dark (Figure 1B and F). The final corrected FD map was generated after masking out areas of projection artifacts from overlying retinal vasculature,[40] and removal of FDs that are sub-physiologic in size, i.e. less than the normal

inter-capillary distance (ICD) (Figure 1C, G).[34] Finally, quantitative analysis was performed on the corrected map.

Three quantitative metrics were defined for each image: FD number (FDN), mean FD size (MFDS) and FD density (FDD) (Figure 1J). FDN is defined as the total number of all individual FDs identified per image, and MFDS is defined as the mean size (μm^2) of all individual FDs identified per image. FDD is defined as a unit-less ratio of the total area occupied by CC FDs divided by the total image area (minus projection artifacts).

Determination of coefficient of variation

Five control subjects and five subjects with posterior uveitis were scanned three times at the same visit using both the 3×3 mm and the 6×6 mm scans. Three of the posterior uveitis patients had the diagnosis of birdshot chorioretinopathy and the other two had the diagnosis of serpiginous choroiditis. Repeatability was calculated for each quantitative metric, FDN, MFDS, FDD and reported as the coefficient of variation (CV).[41]

Statistical analysis

Statistical analyses were performed using MATLAB (R2016b; MathWorks, Inc, Natick, Massachusetts, USA) and Prism (GRAPHPAD software, San Diego, CA, USA). Cohort data are expressed using the median and interquartile range (IQR). Mann-Whitney U-test and Kruskal-Wallis test were used to compare control and uveitis cohorts, p values less than 0.05 were considered significant, in the case of multiple comparisons, Bonferroni correction was performed such that p values less than 0.05/N were considered significant, where N was the number of comparisons made. Non-parametric Spearman correlation was used for correlation testing of groups with non-normal distributions. The receiver operating characteristic (ROC) curve was plotted and the area under the curve (AUC) was calculated to compare the diagnostic power of each metric.

Results

A total of 78 uveitis subjects and 38 controls were recruited and imaged. Five uveitic subjects were excluded: 3 due to the presence of macular edema and 2 due to insufficient scan quality. No control subjects were excluded. For the remaining subjects, both eyes of 73 uveitis patients and 38 controls were imaged and examined. One eye per subject was selected for further analysis as described in methods. The average age of uveitis patients was 49 years and the majority were women (71%). Similar age and gender distribution were present in the control group (Table 1). In the uveitis group, the majority of patients were diagnosed with posterior uveitis (n=40, 54.8%), but patients with anterior uveitis (n=20, 27.4%), intermediate (n=8, 11.0%) and panuveitis (n=5, 6.8%) were also represented.

Choriocapillaris Flow Deficit Analysis in Uveitis and Healthy Controls

222 *en face* CC images were generated from the 3×3 mm and 6×6 mm scans of the 111 study eyes. Representative CC *en face* slabs from control and uveitis subjects are shown in Figure 2. The FD maps for control subjects reveal numerous, small, relatively evenly spaced FDs throughout the macula. Images from uveitis patients demonstrated a range of findings.

For example, images from patients with anterior and intermediate uveitis lacked qualitative lesions, and appeared similar to controls (Figure 2E–H). In contrast, in patients with posterior uveitis, abnormalities of the FD map were grossly apparent. In a patient with Vogt-Koyanagi-Harada disease (VKH), multiple enlarged FDs can be appreciated on both the 3×3mm and 6 ×6mm images (Figure 2I–L). An additional example is provided by a patient with multifocal choroiditis that demonstrates large areas of abnormal flow signal consistent with widespread loss of the CC (Figure 2M–P).

To determine the differences between control and uveitic eyes quantitatively, the three CC flow metrics, FDN, MFDS and FDD, were compared between the control and uveitis groups. Prior to intergroup comparisons, metric repeatability was established using a subset of both controls and uveitis images. CVs ranged from 1.29% to 6.65% (Table 2), with MFDS having the lowest CV among the three metrics (Table 2). The summary of the results for each metric in the uveitis and normal controls are presented in Table 3. In controls, the median FDN is 417 (IQR: 123) per 3×3 mm image and 2365 (IQR: 681) per 6×6 mm image. No significant differences in FDN were identified between control and uveitis patients. In controls, the median MFDS was 751.7 μm^2 (IQR: 69.6 μm^2) per 3×3mm image and 802.0 μm^2 (IQR: 42.1 μm^2) per 6×6 mm image. In uveitis images, the median MFDS was significantly larger than controls in both scan sizes: per 3×3 mm (median: 838.4 μm^2, IQR: 310.2 μm^2, $p<0.0001$) and 6×6 mm (median: 870.9 μm^2, IQR: 274.1 μm^2, $p<0.0001$). Uveitis patients also demonstrated a significantly higher FDD when compared to controls (3×3 mm: $p=0.0002$, 6×6 mm: $p=0.0076$). Thus, our analysis revealed that CC FDs were larger and more densely clustered in the uveitis patients than in controls.

Uveitis Subgroup Analysis

To further investigate the presence of CC abnormality in different types of uveitis, we divided the uveitis cohort into two groups; group A (N=42) without choroidal involvement and group B (N=31) with choroidal involvement (Table 4).[42–45] Group A included diagnoses such as idiopathic anterior uveitis, HLA-B27 associated anterior uveitis, idiopathic intermediate uveitis, idiopathic anterior uveitis associated with MS, Fuchs heterochromic iridocyclitis, Possner-Schlossman syndrome, Susacs syndrome, idiopathic retinal vasculitis, and autoimmune retinopathy. Group B included the diagnoses with choroidal involvement such as birdshot chorioretinopathy, multifocal choroiditis with and without panuveitis, punctate inner choroiditis, Sarcoidosis, serpiginous choroiditis, panuveitis, ampiginous choroiditis and VKH. The two uveitis groups, A and B, were compared to each other and to normal controls.

After subdivision, the impact of the location of inflammation on quantitative parameters became apparent (Figure 3 and Table 5). In uveitis group B (posterior and panuveitis), the median MFDS increased to 1108 μm^2 on 3×3 mm images and to 1104 μm^2 on 6×6 mm images. These values remained significantly larger than normal controls ($p<0.0001$). Conversely, in uveitis group A (anterior and intermediate uveitis), the MFDS decreased to 784 μm^2 on 3×3 mm images and to 820 μm^2 for 6×6 mm images. These values were no longer significantly different from controls ($p=0.0339$ for 3×3 mm images, $p=0.0239$ for 6×6 mm images, significant level $a= 0.017$ with Bonferroni correction). FDD was also

significantly higher in uveitis group B when compared to uveitis group A and normal controls ($p<0.0001$). FDN was not significantly different between groups. In summary, these data show that uveitis patients with choroidal involvement have FDs that are both larger and more densely clustered than uveitis patients without choroidal involvement and normal controls. The number of scans obtained in patients with disease activity noted by the clinician on the date of imaging is also reported in Table 4. In total 26 (35%) of the patients imaged had active uveitis (N=14, 33% group A, N= 12, 39% group B).

The impact of scan-pattern size on quantitative choriocapillaris analysis

In this study we used two scan-patterns, 3×3 mm and 6×6 mm. For each scan pattern there is a different digital resolution and signal to noise ratio (SNR) which has the potential to impact the quantitative results. The 3×3 mm scans provide a higher SNR (3×3 mm uses 4 repeated B-scans) and scanning density (10μm/pixel), and may be more sensitive to small variations in FD size. The 6×6 mm scans provide access to larger regions of the posterior pole, but at the cost of digital resolution (12μm/pixel) and SNR (6×6 mm uses 2 repeated B-scans). To determine which scanning size and quantitative parameter has the best ability to differentiate uveitis group B from controls, we assessed the AUC generated by the ROC for each possible combination of test and scan patterns (Figure 4). In both 3×3 mm and 6×6 mm images, MFDS could best differentiate uveitis group B from controls (3×3, AUC = 0.9480; 6×6, AUC = 0.9714). FDD also demonstrated good discrimination ability in both scan sizes, (3×3 AUC = 0.8505 and 6×6, AUC = 0.8093). FDN was not able to differentiate uveitis group B from controls in either 3×3 mm (fail, AUC 0.5733) or 6×6 mm (fail, AUC = 0.4429) images.

To further investigate the relationship between quantitative CC analyses in the two scanning sizes, we conducted non-parametric Spearman correlation for all three FD metrics (Figure 5). Significant correlation (all $p<0.0001$) was observed in all three metrics, with MFDS demonstrating the strongest correlation among all (Figure 5C, $r = 0.8026$), followed by FDD (Figure 5A, $r = 0.5072$) and FDN (Figure 5B, $r = 0.388$). These results indicate that even though 3×3 mm and 6×6 mm scans have different discriminative powers as demonstrated by the ROC data, each of the FD measurements are still significantly correlated and are good at identifying uveitis group B from controls.

Discussion

In this study, we utilized a combination of the commercially available SS-OCTA *en face* CC images and a novel automated algorithm to automatically identify and quantify CC FDs in patients with uveitis. Using this unbiased, objective approach, we found that the FDs in patients with uveitis are larger in size and occur at a higher density than FDs of normal controls. Furthermore, after subdividing the uveitis cohort into two groups based on the absence (uveitis group A) or presence of choroidal involvement (uveitis group B), we were able to refine the scope of our findings. Not surprisingly, the subgroup analysis found that in the absence of known choroidal disease, CC FDs in uveitis patients were not significantly different from controls. In contrast, in patients with posterior or panuveitis, where the choroid is the main site of inflammation, CC FDs were significantly larger and present in

higher density than FDs in both normal controls and patients with anterior segment inflammation.

Quantitative analysis of CC blood flow presents different challenges than similar analyses of retinal vascular blood flow, including OCT signal attenuation, signal scattering though the RPE/BM complex and the high degree of lateral resolution required to accurately resolve CC structure.[46] Moving from SD-OCTA to SS-OCTA has made choroidal anatomy more accessible and improved the quality of images for quantitative analysis, but high quality, high resolution images are still difficult to obtain. In this study, we utilized a post-acquisition image processing approach to address these on-going challenges. Our approach uses a combination of complex thresholding that is sensitive to the intrinsic histogram of each image,[47] elimination of sub-physiologic size FDs,[34] structural compensation for possible signal attenuation due to RPE,[33] and removal of projection artifacts[40] to improve image quality and decrease interscan CV. We believe these post-processing steps are necessary given the current stage of technology deployed in commercially available SS-OCTA systems. Our results here indicate that this approach is useful and can produce results with good repeatability.

One of the benefits of quantitative image analysis is that it can provide an objective measurement of clinically relevant parameters of choroidal blood flow for longitudinal monitoring. Quantitative metrics of the retinal vasculature have been developed that describe the length, density, or branching patterns of the vessels and these metrics have been used to define characteristics of the retinal vasculature in healthy and diseased eyes.[2–4, 48, 49] In contrast to the approach used to define retinal blood flow, terms defining CC blood flow have been developed that describe the areas without blood flow. This convention was adopted partially because normal CC vasculature cannot be completely resolved by commercial OCTA systems. Common OCTA lateral resolution (~15–20 μm) is larger than common CC ICD in the posterior pole (5–20 μm),[50] but smaller than the ICD in the retina (71.30 ± 5.17 μm).[51] Therefore, the most striking features in the CC *en face* images obtained from a normal eye are the small dark spots that represent the absence of detectable flow rather than the normal CC vasculature. In eyes with posterior segment pathology, the dark spots tend to match areas of pathology defined by other standard of care clinical imaging modalities.[15, 24] The terminology for these dark spots has not been firmly established, but they have been termed FDs, flow voids, or flow signal voids.[33–35, 38, 52] We favor the term FD as the OMAG algorithm used to generate flow data is based on the movement of red blood cells. Thus, the absence of a flow signal is most likely to represent a *deficit* of red blood cell *flow*.

We chose to use three previously published quantitative metrics to summarize and compare the images in this study: total FDN, MFDS, and FDD.[53] We found that patients with posterior uveitis have significantly larger MFDS and higher FDD when compared to both normal controls and uveitis patients without posterior involvement. Furthermore, this pattern held true for images from both the 3×3 mm and 6×6 mm scans. Quantitative metrics that are robust when applied to high resolution foveal scans, as well as larger size scanning patterns, will be important for use in diseases such as uveitis that often have pathology extending throughout and beyond the central macula. Furthermore, the ROC analysis suggests that

even though the 3×3 mm scans outperform the 6×6 mm scans using FDD (3×3 mm: AUC = 0.8505, 6×6 mm: AUC = 0.8093), the 6×6 mm scans are better than the 3×3 mm scans for detecting pathology in patients with uveitis when using MFDS as the indicator of disease (3×3 mm: AUC = 0.9480, 6×6 mm: AUC = 0.9714). It is not uncommon that OCTA parameters calculated using different scan sizes result in different diagnostic powers.[54] We suspect one reason for the differences in this study is the size and location of CC pathology in relationship to the area of the macula covered by the different area that is imaged. Some pathology was not contained within or could not be fully captured by the 3×3 mm scans. Another potential factor is the higher digital resolution of the 3×3 mm scans. The 3×3 mm OCTA images are generated using four repeated B-scans to generate OCTA data and have a lateral spacing of 10 μm/pixel. In contrast, 6×6 mm scans use two repeated B-scans to generate OCTA data with a lateral spacing of 12 μm/pixel. Thus, 3×3 mm scans may be more sensitive to small or subtle differences in FDs while 6×6 mm scans are better at detecting pathology that generates less subtle (i.e. large) FD changes that are common in patients with posterior uveitis. Clinical exams will almost always be sufficient for making a uveitis diagnosis, and it is unlikely that CC FD metrics would be indicated as a diagnostic test. However, there are forms of posterior uveitis that mimic age-related macular degeneration (ARMD), and it is possible that differences in MFDS could help differentiate less common causes of a choroidal neovascular membrane, like posterior placoid choroiditis or punctate inner choroiditis, from ARMD.

In this study, the fully automated process of CC quantification followed the commercially available process and device specific process for generating the CC OCTA image. Since this was a research-based proof of concept study, we did not exclude images generated by the device specific software if they had gross segmentation errors. Instead, we corrected the segmentation manually prior to quantitative analysis. Accurate CC slab generation using OCTA relies heavily on accurate identification of the RPE/BM complex. While commercial systems perform well when segmenting healthy eyes, automated RPE segmentation in eyes with pathology at the level of the RPE can be more challenging.[55] Ultimately, for this approach to become clinically accessible, it would require full and reliable automation at all stages of image acquisition and analyses. Optimization of segmentation performance in eyes with pathology at the level of the RPE is on-going and necessary for realization of the goal for fully automated analysis.

There are a number of limitations to our automated approach. Most importantly, signal strength has an impact on reproducibility of FD identification. We used a highly curated data set here that represents images with a signal strength of 8 or higher. Due to many possible causes of media opacity in patients with uveitis, these high-quality scans are not always achievable. However, we were able to achieve this level of scan quality in 26 of the 31 active uveitis patients recruited to this study (5 that were imaged were excluded from the study). This success may not be typical since we did not recruit all sequential patients seen in clinic, and our success in imaging these patients is likely impacted by selection bias. This study is also limited by the small number of patients imaged with each specific diagnosis. Due to our small sample size, we divided our entire uveitis cohort into two groups based on the presence or absence of choroidal involvement rather than each individual diagnosis. This design allowed us to make conclusions about the performance of our automated image

analysis approach in detecting the presence and extent of CC pathology, but does not allow us to make disease specific conclusions. Future studies with larger sample sizes are certainly warranted to determine the clinical relevance of this type of image analysis to specific forms of posterior uveitis. Lastly, our study cohort is cross-sectional and lacks longitudinal scans. Thus, we did not perform an analysis to correlate disease activity with quantitative FD parameters. Despite these limitations, we were able to demonstrate that reliable, automated, quantitative CC assessment could identify significant differences in clinically distinct uveitis populations.

In summary, this study demonstrates that a fully automated image analysis process is reliable and can be used to generate unbiased quantitative metrics of CC pathology in eyes with posterior uveitis. This method for automated and quantitative analysis of CC FDs could be developed into a non-invasive clinical tool for monitoring patients with posterior uveitis.

Acknowledgments

a. **Funding/Support:** Research supported by grants from the National Eye Institute (NEI K08EY023998, R01 EY024158 and R01 EY028753), the Cynthia and Joseph Gensheimer Fellowship, Research to Prevent Blindness Career Development Award, Carl Zeiss Meditec, and an unrestricted Departmental Grant from Research to Prevent Blindness. The funding organization had no role in the design or conduct of this research.

b. **Financial Disclosures:** Dr. Wang received research support from Carl Zeiss Meditec, Inc.

Dr. Wang discloses intellectual property owned by the Oregon Health and Science University and the University of Washington. Dr. Wang also receives research support from Tasso Inc, Moptim Inc, Colgate Palmolive Company and Facebook technologies LLC. He is a consultant to Insight Photonic Solutions, Kowa, and Carl Zeiss Meditec.

The remaining authors have no disclosures.

References

1. Spaide RF, Klancnik JM, Cooney MJ. Retinal vascular layers imaged by fluorescein angiography and optical coherence tomography angiography. JAMA ophthalmology 2015;133:(1):45–50. [PubMed: 25317632]
2. Koulisis N, Kim AY, Chu Z, et al. Quantitative microvascular analysis of retinal venous occlusions by spectral domain optical coherence tomography angiography. PLoS ONE 2017;12:(4):e0176404. [PubMed: 28437483]
3. Kim AY, Rodger DC, Shahidzadeh A, et al. Quantifying Retinal Microvascular Changes in Uveitis Using Spectral-Domain Optical Coherence Tomography Angiography. Am J Ophthalmol 2016;171:101–112. [PubMed: 27594138]
4. Kim AY, Chu Z, Shahidzadeh A, Wang RK, Puliafito CA, Kashani AH. Quantifying Microvascular Density and Morphology in Diabetic Retinopathy Using Spectral-Domain Optical Coherence Tomography AngiographyQuantifying Vascular Changes in DR With SD-OCTA. Invest Ophthalmol Vis Sci 2016;57:(9):OCT362–OCT370. [PubMed: 27409494]
5. Chu Z, Lin J, Gao C, et al. Quantitative assessment of the retinal microvasculature using optical coherence tomography angiography. J Biomed Opt 2016;21:(6):066008–066008.
6. Waizel M, Todorova MG, Terrada C, LeHoang P, Massamba N, Bodaghi B. Superficial and deep retinal foveal avascular zone OCTA findings of non-infectious anterior and posterior uveitis. Graefes Arch Clin Exp Ophthalmol 2018;256:(10):1977–1984. [PubMed: 29980918]
7. Spaide RF, Klancnik JM Jr, Cooney MJ. REtinal vascular layers in macular telangiectasia type 2 imaged by optical coherence tomographic angiography. JAMA Ophthalmology 2015;133:(1):66–73. [PubMed: 25317692]

8. Hwang TS, Jia Y, Gao SS, et al. Optical coherence tomography angiography features of diabetic retinopathy. Retina (Philadelphia, Pa) 2015;35:(11):2371.

9. Thorell MR, Zhang Q, Huang Y, et al. Swept-source OCT angiography of macular telangiectasia type 2. Ophthalmic Surgery, Lasers and Imaging Retina 2014;45:(5):369–380.

10. Hassan M, Agarwal A, Afridi R, et al. The role of optical coherence tomography angiography in the Management of Uveitis. Int Ophthalmol Clin 2016;56:(4):1–24.

11. Talisa E, Bonini Filho MA, Adhi M, Duker JS. Retinal and choroidal vasculature in birdshot chorioretinopathy analyzed using spectral domain optical coherence tomography angiography. Retina 2015;35:(11):2392–2399. [PubMed: 26352557]

12. Khairallah M, Abroug N, Khochtali S, et al. Optical coherence tomography angiography in patients with Behcet uveitis. Retina 2017;37:(9):1678–1691. [PubMed: 28002270]

13. Pichi F, Sarraf D, Arepalli S, et al. The application of optical coherence tomography angiography in uveitis and inflammatory eye diseases. Prog Retin Eye Res 2017;59:178–201. [PubMed: 28465249]

14. Graham E, Stanford M, Shilling J, Sanders M. Neovascularisation associated with posterior uveitis. Br J Ophthalmol 1987;71:(11):826–833. [PubMed: 2446653]

15. Pakzad-Vaezi K, Khaksari K, Chu Z, Van Gelder RN, Wang RK, Pepple KL. Swept-Source OCT Angiography of Serpiginous Choroiditis. Ophthalmology Retina 2018;2:(7):712–719. [PubMed: 30148243]

16. Howes EL, Cruse VK. The structural basis of altered vascular permeability following intraocular inflammation. Arch Ophthalmol 1978;96:(9):1668–1676. [PubMed: 687212]

17. Nazari H, Hariri A, Hu Z, Ouyang Y, Sadda S, Rao NA. Choroidal atrophy and loss of choriocapillaris in convalescent stage of Vogt-Koyanagi-Harada disease: in vivo documentation. Journal of ophthalmic inflammation and infection 2014;4:(1):9. [PubMed: 24655594]

18. Aggarwal K, Agarwal A, Mahajan S, et al. The Role of Optical Coherence Tomography Angiography in the Diagnosis and Management of Acute Vogt–Koyanagi–Harada Disease. Ocul Immunol Inflamm 2018;26:(1):142–153. [PubMed: 27440118]

19. Borrelli E, Souied EH, Freund KB, et al. Reduced choriocapillaris flow in eyes with type 3 neovascularization and age-related macular degeneration. Retina 2018;38:(10):1968–1976. [PubMed: 29746411]

20. Klufas MA, Phasukkijwatana N, Iafe NA, et al. Optical coherence tomography angiography reveals choriocapillaris flow reduction in placoid chorioretinitis. Ophthalmology Retina 2017;1:(1):77–91. [PubMed: 31047399]

21. Spaide RF. Choriocapillaris flow features follow a power law distribution: implications for characterization and mechanisms of disease progression. Am J Ophthalmol 2016;170:58–67. [PubMed: 27496785]

22. Xu J, Song S, Men S, Wang RK. Long ranging swept-source optical coherence tomography-based angiography outperforms its spectral-domain counterpart in imaging human skin microcirculations. J Biomed Opt 2017;22:(11):116007.

23. Zhang Q, Rezaei KA, Saraf SS, Chu Z, Wang F, Wang RK. Ultra-wide optical coherence tomography angiography in diabetic retinopathy. Quantitative imaging in medicine and surgery 2018;8:(8):743. [PubMed: 30306055]

24. Pepple KL, Chu Z, Weinstein J, Munk MR, Van Gelder RN, Wang RK. Use of En Face Swept-Source Optical Coherence Tomography Angiography in Identifying Choroidal Flow Voids in 3 Patients With Birdshot Chorioretinopathy. JAMA ophthalmology 2018;136:(11):1288–1292. [PubMed: 30128478]

25. Cheung CMG, Yanagi Y, Mohla A, et al. Characterization and differentiation of polypoidal choroidal vasculopathy using swept source optical coherence tomography angiography. Retina 2017;37:(8):1464–1474. [PubMed: 27828911]

26. Jung JJ, Chen MH, Chung PY, Lee SS. Swept-source optical coherence tomography angiography for choroidal neovascularization after bevacizumab and photodynamic therapy. American Journal of Ophthalmology Case Reports 2016;1:1–4. [PubMed: 29503879]

27. Byon I, Nassisi M, Borrelli E, Sadda SR. Impact of Slab Selection on Quantification of Choriocapillaris Flow Deficits by Optical Coherence Tomography Angiography. Am J Ophthalmol 2019;208:397–405. [PubMed: 31493401]
28. Group SoUNW. Standardization of uveitis nomenclature for reporting clinical data. Results of the First International Workshop. Am J Ophthalmol 2005;140:(3):509–516. [PubMed: 16196117]
29. Meditec CZ. Carl Zeiss Meditec Plex Elite 9000 OCT 501(k) premarket report of FDA, 2016.
30. Nassisi M, Shi Y, Fan W, et al. Choriocapillaris impairment around the atrophic lesions in patients with geographic atrophy: a swept-source optical coherence tomography angiography study. Br J Ophthalmol 2018;103:(7):911–917. [PubMed: 30131381]
31. Gorczynska I, Migacz J, Jonnal R, Zawadzki R, Poddar R, Werner J. Imaging of the human choroid with a 1.7 MHz A-scan rate FDML swept source OCT system. Proc. of SPIE Vol, 2017:1004510–1004511.
32. Wang RK. Optical microangiography: a label-free 3-D imaging technology to visualize and quantify blood circulations within tissue beds in vivo. IEEE Journal of Selected Topics in Quantum Electronics 2010;16:(3):545–554. [PubMed: 20657761]
33. Zhang Q, Zheng F, Motulsky EH, et al. A Novel Strategy for Quantifying Choriocapillaris Flow Voids Using Swept-Source OCT Angiography. Invest Ophthalmol Vis Sci 2018;59:(1):203–211. [PubMed: 29340648]
34. Chu Z, Zhou H, Cheng Y, Zhang Q, Wang RK. Improving visualization and quantitative assessment of choriocapillaris with swept source OCTA through registration and averaging applicable to clinical systems. Scientific reports 2018;8:(1):16826. [PubMed: 30429502]
35. Zhang Q, Shi Y, Zhou H, et al. Accurate estimation of choriocapillaris flow deficits beyond normal intercapillary spacing with swept source OCT angiography. Quantitative imaging in medicine and surgery 2018;8:(7):658. [PubMed: 30211033]
36. Rochepeau C, Kodjikian L, Garcia M-A, et al. Optical Coherence Tomography Angiography Quantitative Assessment of Choriocapillaris Blood Flow in Central Serous Chorioretinopathy. Am J Ophthalmol 2018;194:26–34. [PubMed: 30053475]
37. Al-Sheikh M, Phasukkijwatana N, Dolz-Marco R, et al. Quantitative OCT angiography of the retinal microvasculature and the choriocapillaris in myopic eyes. Invest Ophthalmol Vis Sci 2017;58:(4):2063–2069. [PubMed: 28388703]
38. Zheng F, Zhang Q, Shi Y, et al. Age-dependent Changes in the Macular Choriocapillaris of Normal Eyes Imaged With Swept-Source Optical Coherence Tomography Angiography. Am J Ophthalmol 2019;200:110–122. [PubMed: 30639367]
39. Spaide RF, Fujimoto JG, Waheed NK, Sadda SR, Staurenghi G. Optical coherence tomography angiography. Prog Retin Eye Res 2018;64:1–55. [PubMed: 29229445]
40. Zhang Q, Zhang A, Lee CS, et al. Projection artifact removal improves visualization and quantitation of macular neovascularization imaged by optical coherence tomography angiography. Ophthalmology retina 2017;1:(2):124–136. [PubMed: 28584883]
41. Bland JM, Altman DG. Measurement error proportional to the mean. BMJ 1996;313:(7049):106. [PubMed: 8688716]
42. Cao JH, Silpa-Archa S, Freitas-Neto CA, Foster CS. Birdshot chorioretinitis lesions on indocyanine green angiography as an indicator of disease activity. Retina 2016;36:(9):1751–1757. [PubMed: 26977742]
43. Bouchenaki N, Cimino L, Auer C, Tran VT, Herbort CP. Assessment and classification of choroidal vasculitis in posterior uveitis using indocyanine green angiography. Klin Monatsbl Augenheilkd 2002;219:(04):243–249. [PubMed: 12022010]
44. Howe L, Stanford M, Graham E, Marshall J. Indocyanine green angiography in inflammatory eye disease. Eye 1998;12:(5):761. [PubMed: 10070505]
45. Rao NA. Pathology of Vogt–Koyanagi–Harada disease. Int Ophthalmol 2007;27:(2–3):81–85. [PubMed: 17435969]
46. Lauermann JL, Eter N, Alten F. Optical coherence tomography angiography offers new insights into choriocapillaris perfusion. Ophthalmologica 2018;239:(2–3):74–84. [PubMed: 29353272]

47. Wang Q, Chan S, Yang JY, et al. Vascular density in retina and choriocapillaris as measured by optical coherence tomography angiography. Am J Ophthalmol 2016;168:95–109. [PubMed: 27183862]

48. Richter GM, Madi I, Chu Z, et al. Structural and Functional Associations of Macular Microcirculation in the Ganglion Cell-Inner Plexiform Layer in Glaucoma Using Optical Coherence Tomography Angiography. J Glaucoma 2018;27:(3):281–290. [PubMed: 29394201]

49. Jia Y, Bailey ST, Hwang TS, et al. Quantitative optical coherence tomography angiography of vascular abnormalities in the living human eye. Proceedings of the National Academy of Sciences 2015;112:(18):E2395–E2402.

50. Olver J Functional anatomy of the choroidal circulation: methyl methacrylate casting of human choroid. Eye 1990;4:(2):262–272. [PubMed: 2379644]

51. Chan G, Balaratnasingam C, Xu J, et al. In vivo optical imaging of human retinal capillary networks using speckle variance optical coherence tomography with quantitative clinico-histological correlation. Microvascular research 2015;100:32–39. [PubMed: 25917012]

52. Matet A, Daruich A, Hardy S, Behar-Cohen F. PATTERNS OF CHORIOCAPILLARIS FLOW SIGNAL VOIDS IN CENTRAL SEROUS CHORIORETINOPATHY: An Optical Coherence Tomography Angiography Study. Retina 2018;39:(11):2178–2188.

53. Chu Z, Chen Y, Zhang Q, et al. Accurate visualization and quantification of choriocapillaris with swept source OCTA through averaging repeated volume scans. Invest Ophthalmol Vis Sci 2018;59:(9):2880–2880. [PubMed: 30025134]

54. Chang R, Chu Z, Burkemper B, et al. Effect of Scan Size on Glaucoma Diagnostic Performance using OCT Angiography En Face Images of the Radial Peripapillary Capillaries. J Glaucoma 2019; 28:(5):465–472. [PubMed: 30789527]

55. Borrelli E, Shi Y, Uji A, et al. Topographic Analysis of the Choriocapillaris in Intermediate Age-related Macular Degeneration. Am J Ophthalmol 2018;196:34–43. [PubMed: 30118688]

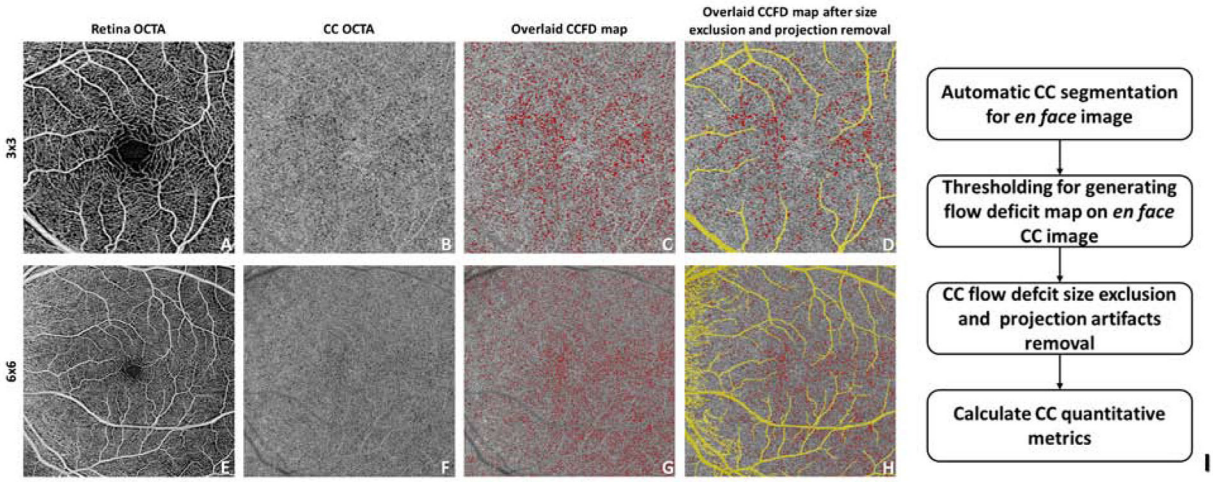

Figure 1.

Automated detection and quantification of choriocapillaris (CC) flow deficits from en face swept-source optical coherence tomography angiography images. The diagram shows an example of our proposed CC analysis in a normal patient with both 3×3 mm (A-D) and 6×6 mm (E-H) scans. I: flow chart of the proposed CC analysis.

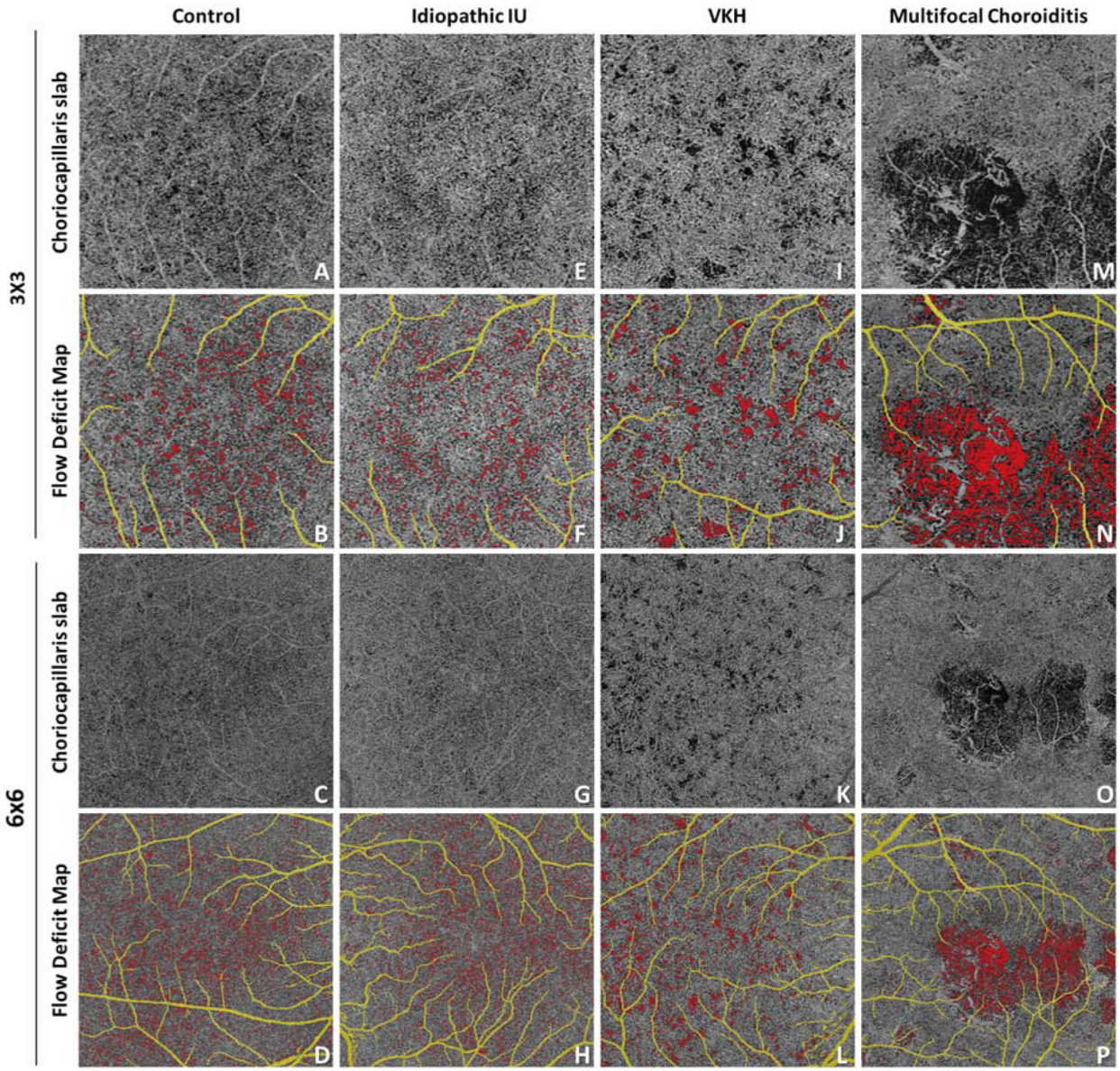

Figure 2.

Automated detection of flow deficits (FDs) in control and uveitis. For uveitis, examples are idiopathic intermediate uveitis, Vogt-Koyanagi-Harada disease and multifocal choroiditis. A, E, I, M: optical coherence tomography angiography (OCTA) choriocapillaris (CC) slab in 3×3 mm scans; B, F, J, N: computed FD map in 3×3 mm scans, with FDs color coded in red, retinal projection artifacts color coded in yellow; C, C, K, O: OCTA CC slab in 6×6 mm scans; D, H, L, P: computed FD map in 6×6 mm scans, with FDs color coded in red, retinal projection artifacts color coded in yellow;

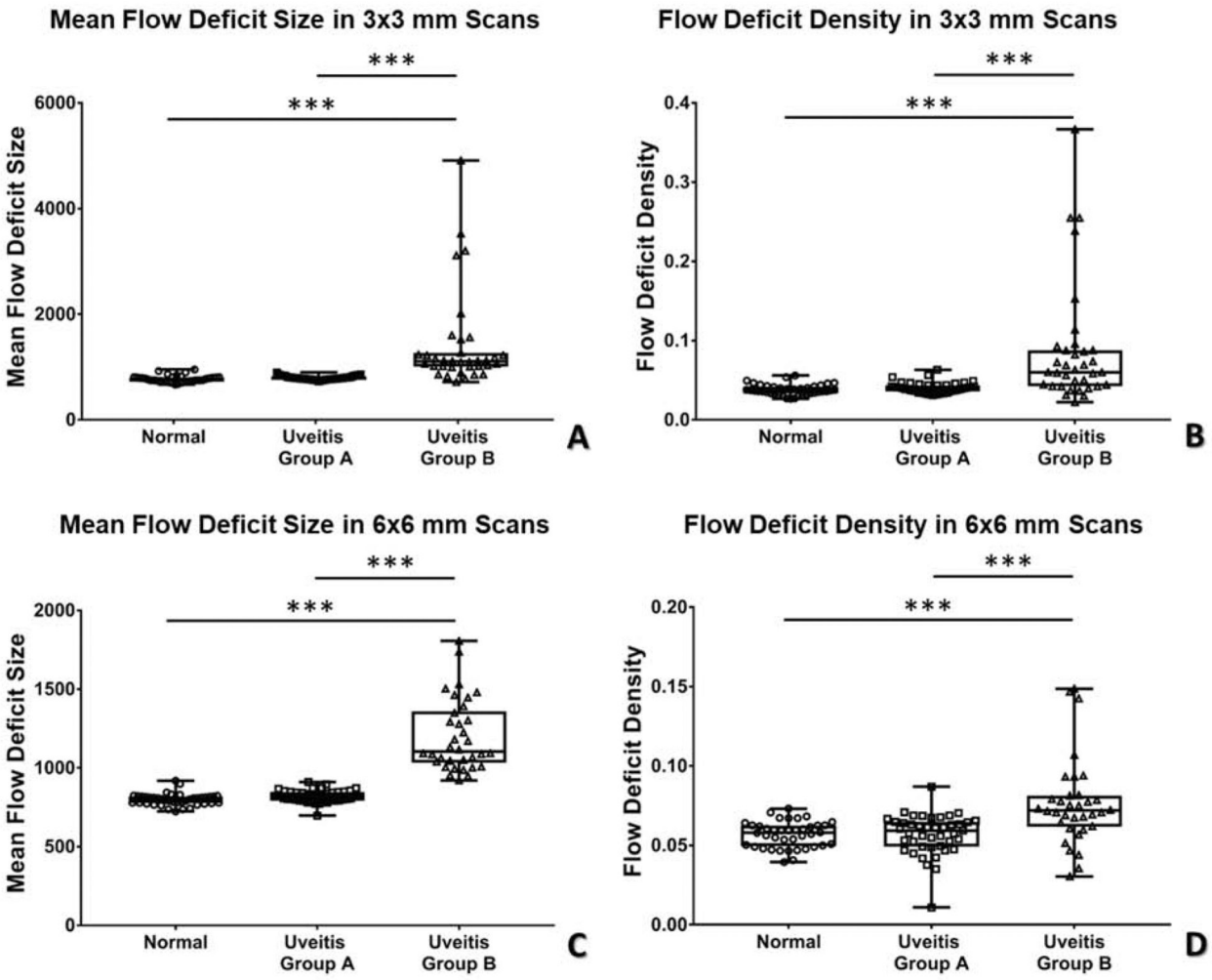

Figure 3.

Scatter plot of flow deficit density (FDD) and mean flow deficit size (MFDS) in uveitis subgroups and controls in both 3×3 mm and 6×6 mm scans. A: MFDS in 3×3 mm scans; B: FDD in 3×3 mm scans; C: MFDS in 6×6 mm scans, D: FDD in 6×6 mm scans.

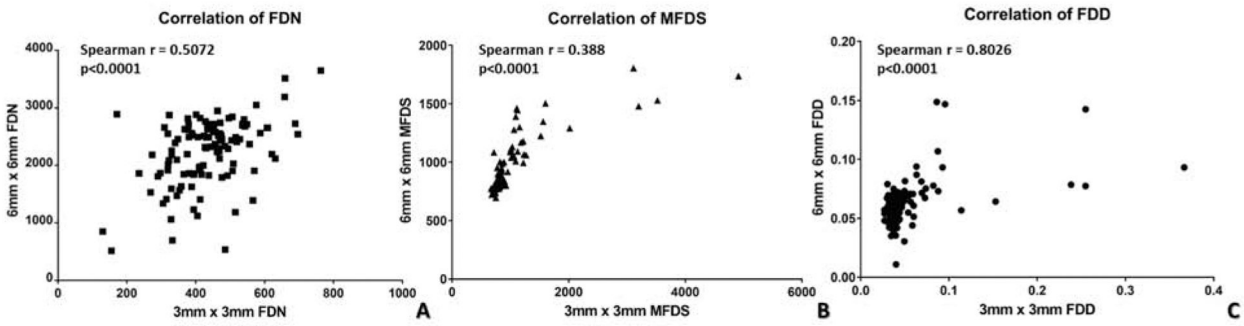

Figure 4.

Nonparametric Spearman correlation of 3×3 mm and 6×6 mm scans for quantitative choriocapillaris metrics. A: Spearman correlation of 3×3 mm and 6×6 mm scans with flow deficit number; B: Spearman correlation of 3×3 mm and 6×6 mm scans with mean flow deficit size; C: Spearman correlation of 3×3 mm and 6×6 mm scans with flow deficit density.

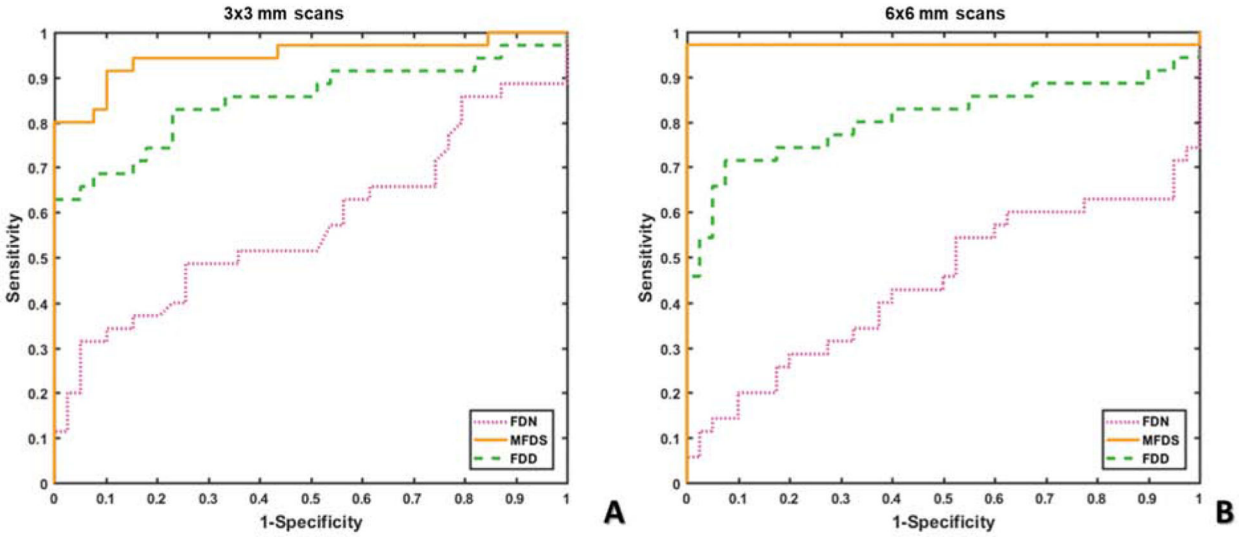

Figure 5.

Receiver operating characteristic (ROC) curves of all choriocapillaris (CC) quantitative metrics. A: ROC curves of all CC quantitative metrics in 3×3 mm scans; B: ROC curves of all CC quantitative metrics in 6×6 mm scans; (flow deficit number = FDN, mean flow deficit size = MFDS and flow deficit density = FDD).

Table 1.

Patient demographics. Age is represented as mean±standard deviation (range)

	Control	Uveitis		P value
Number	38	73		NA
Age	54±22 (32–76)	49±15 (22–75)		0.221
Female percentage	53%	71%		0.057
Anatomic classification		Anterior	20	NA
		Intermediate	8	NA
		Posterior	40	NA
		Panuveitis	5	NA

Table 2.

Intra-visit repeatability of proposed choriocapillaris analysis.

CV	FDN	MFDS (μm^2)	FDD
3×3 mm Control	5.06%	2.58%	4.17%
3×3 mm Uveitis	6.57%	5.57%	6.65%
6×6 mm Control	3.85%	1.29%	3.79%
6×6 mm Uveitis	5.00%	4.29%	4.72%

Abbreviations: CV, coefficient of variation; FDN, flow deficit number; MFDS, mean flow deficit size; FDD, flow deficit density.

Table 3.

Quantitative analysis of choriocapillaris flow metrics in uveitis and controls.

Median (IQR)	3×3			6×6		
	FDN	MFDS (μm^2)	FDD	FDN	MFDS (μm^2)	FDD
Control	417 (123)	751.74 (69.64)	0.037 (0.008)	2365 (681)	802.02 (42.13)	0.058 (0.013)
Uveitis	442 (141)	838.36 (310.25)	0.042 (0.023)	2323 (829)	870.93 (274.14)	0.063 (0.018)
Mann-Whitney U-test	p=0.1061	p<0.0001*	p=0.0002*	p=0.6917	p<0.0001*	p=0.0076*

Abbreviations: IQR, interquartile range; FDN, flow deficit number; MFDS, mean flow deficit size; FDD, flow deficit density.

Table 4.

Subgroup of uveitis patients by choroidal involvement.

	Uveitis without choroidal involvement (Group A)		Uveitis with choroidal involvement (Group B)	
Number	N=42 (Active=14, 33%)		N=31 (12, 39%)	
	Idiopathic AU	12 (6)	Birdshot Chorioretinopathy	13 (4)
	Retinal vasculitis	9 (0)	Multifocal Choroiditis	6 (1)
	Idiopathic IU	7 (6)	Serpiginous Choroiditis	4 (3)
	Idiopathic IU associated with MS	1 (0)	Multifocal Choroiditis and Panuveitis	2 (1)
	HLA-B27	6 (1)	Ampiginous Choroiditis	1 (1)
	Susacs Syndrome	3 (0)	Punctate Inner Choroiditis	2 (0)
	Autoimmune Retinopathy	2 (1)	Vogt-Koyanagi-Harada Disease	1 (1)
	Fuchs iriodcyclitiis	1 (0)	Sarcoidosis	1 (1)
	Posner-Schlossman Syndrome	1 (0)	Panuveitis	1 (0)

The total number of patients per group are listed for each diagnosis. The number in parentheses indicates the number of patients with disease activity at the time of imaging.

Table 5.

Quantitative analysis of choriocapillaris flow metrics in patients with uveitis subgroups and controls.

Median (IQR)		**3×3**			**6×6**		
		FDN	**MFDS (μm^2)**	**FDD**	**FDN**	**MFDS (μm^2)**	**FDD**
Normal		417 (123)	751.7 (69.6)	0.037 (0.008)	2365 (681)	802.0 (42.1)	0.058 (0.013)
Uveitis Group A		446 (111)	784.6 (51.1)	0.040 (0.008)	2391 (737)	820.9 (55.7)	0.059 (0.015)
Uveitis Group B		438 (234)	1108.4 (258.4)	0.060 (0.045)	2284 (1251)	1104.5 (328.1)	0.072 (0.020)
Kruskal-Wallis Test (a = 0.05)		p=0.2666	p<0.0001*	p<0.0001*	p=0.4680	p<0.0001*	p<0.0001*
Mann- Whitney U-test (a= 0.017)	**Control: Uveitis Group A**	p=0.2041	p=0.0339	p=0.1428	p=0.9144	p=0.0239	p=0.9357
	Control: Uveitis Group B	p=0.4366	p<0.0001*	p<0.0001*	p=0.2348	p<0.0001*	p<0.0001*
	Uveitis Group A: Uveitis Group B	p=0.9608	p<0.0001*	p<0.0001*	p=0.2028	p<0.0001*	p<0.0001*

Abbreviations: IQR, interquartile range; FDN, flow deficit number; MFDS, mean flow deficit size; FDD, flow deficit density.